PCCP

ROYAL SOCIETY OF CHEMISTRY

PAPER

View Article Online
View Journal | View Issue

Cite this: *Phys. Chem. Chem. Phys.*, 2026, **28**, 9594

Gas-phase spectroscopy of $H_2O@C_{60}^+$ and $H_2O@C_{60}H^+$ in the mid-infrared: the challenges of searching for endohedral fullerenes in space

Olivia O'Neill, [a] Julianna Palotás, †[a] Thomas E. Douglas-Walker, [a] Richard J. Whitby, [b] Malcolm H. Levitt, [b] George R. Bacanu, [b] Cate S. Anstöter, ‡[a] Giel Berden, [cd] Jos Oomens *[cd] and Ewen K. Campbell *[a]

Molecular surgery allows the synthesis of a unique class of molecules known as endohedral fullerenes, where a small species is enclosed within the hollow cavity of a fullerene cage. In this work, mid-IR spectra are presented for the endohedral fullerenes $H_2O@C_{60}^+$ and $H_2O@C_{60}H^+$, obtained using helium tagging spectroscopy and IRMPD spectroscopy, respectively. These are the first gas-phase vibrational spectra of an endohedral fullerene containing an IR-active guest species. Both spectra look remarkably similar to those of the empty fullerenes, with many of the same features present at slightly blue-shifted frequencies. Interestingly, the water bending mode is not observed in either of the spectra. This has been attributed to a polarisation of the π-electrons of the fullerene cage, reducing the total dipole moment and the IR intensities. The similarity of the spectra with those of the empty fullerenes means that these species will be very hard to distinguish using only IR spectroscopy. This may have significant implications for the detection of $H_2O@C_{60}^+$, $H_2O@C_{60}H^+$, or indeed other endohedral fullerenes, in space. The IR emission features of the endohedral fullerene will overlap with those of the empty fullerene, so astronomical detection will need to rely on other spectroscopic techniques.

Received 17th February 2026,
Accepted 24th March 2026

DOI: 10.1039/d6cp00593d

rsc.li/pccp

1 Introduction

Shortly after the serendipitous discovery of fullerenes,[1] the opportunity to isolate a guest species inside the cage was realised. The first endohedral fullerene, La@C_{60}, was reported in 1985, synthesised from laser vaporisation of a La-doped graphite disk.[2] The intra-cavity structure was later proven by the synthesis of the first non-metal endohedral fullerene, He@C_{60}, from collision experiments of helium with C_{60} and C_{70}.[3] To obtain macroscopic quantities of endohedral fullerenes, a synthetic 'molecular surgery' process was developed,[4–6] which involves opening the fullerene, inserting the guest species, and then repairing the hole. This technique facilitates the inclusion of molecules into fullerenes, including H_2,[7] HF,[8] H_2O[9,10] and CH_4.[11] The presence of an endohedral species may alter the structure and reactivity of the fullerene cage, although this is dependent on the interactions between the cage and the encapsulated guest.

The unique, high-symmetry structure of fullerenes means that they are able to survive destructive processes in the interstellar medium, such as photodissociation.[12] Endohedral fullerenes are expected to exhibit a similar resilience.[13] Therefore, given the prevalence of fullerenes in space, the relevance of endohedral fullerenes in cosmic environments should be investigated. Endohedral analogues of both neutral and cationic C_{60} are good candidates due to the detection of C_{60} across a wide range of astrophysical objects[14–17] and the identification of C_{60}^+ as a diffuse interstellar band (DIB) carrier.[18–20] The high proton affinity of C_{60}[21] also suggests that $C_{60}H^+$ analogues could be abundant in interstellar environments and their endohedral derivatives should be considered in the search for extraterrestrial endohedral fullerenes. Endohedral fullerenes possessing cosmically-abundant guest species, such as H_2, He, Fe, Mg, Ca, Na or K, are of particular interest to astrochemistry.[22]

The fullerene cage offers a safe and stable environment for the encapsulated species,[23] which could have important implications

[a] *School of Chemistry, University of Edinburgh, Joseph Black Building, David Brewster Road, Edinburgh, EH9 3FJ, UK. E-mail: e.k.campbell@ed.ac.uk*
[b] *Chemistry, University of Southampton, Southampton, Hants, SO17 1BJ, UK*
[c] *HFML-FELIX, Toernooiveld 7, Nijmegen, 6525 ED, The Netherlands. E-mail: jos.oomens@ru.nl*
[d] *Institute for Molecules and Materials, Radboud University, Heyendaalseweg 135, Nijmegen, 6525 AJ, The Netherlands*
† Stavropoulos Center for Complex Quantum Matter, Department of Physics and Astronomy, University of Notre Dame, Notre Dame, Indiana 46556, USA.
‡ School of Chemistry, University of Glasgow, Joseph Black Building, University Avenue, Glasgow, G12 8QQ, UK.

for interstellar chemistry and the transportation of molecules through space. Though the possibility of endohedral fullerenes existing in space is exciting, evidence of their presence remains elusive. Astronomical detection relies on obtaining gas-phase laboratory data to both compare with observations, and understand how the spectroscopic properties are influenced by the encapsulated guests. There is a scarcity of appropriate laboratory data due to experimental challenges in obtaining the gas-phase spectra of large carbonaceous ions. Advances in laboratory spectroscopy have facilitated the collection of these data *via* techniques such as action spectroscopy.

In conditions simulating stellar outflows, endohedral metallofullerenes have been shown to form as readily as fullerenes.[23] IR spectra have been calculated for a multitude of different metals encapsulated in both neutral and charged C_{60}, revealing substantial differences when compared to the spectrum of the empty cage.[24] Although there are currently no confirmed detections of metallofullerenes in space, their presence has been proposed as a contributing factor in the discrepancies observed in IR band intensity ratios attributed to C_{60}.[24] In comparison, molecular and rare gas endohedrals exhibit much weaker interactions with the cage.[25] For $H_2@C_{60}^+$, the IR spectrum looks very similar to that of C_{60}^+ although some of the features are slightly blue-shifted.[26] Small shifts will be difficult to distinguish in astronomical IR spectra due to the broad widths of the observed C_{60} emission bands. A polar molecule might give rise to more significant interactions with the cage and larger perturbations of the cage vibrations. Moreover, the dipole moment and IR-active modes of encapsulated species, such as H_2O, enable exploration of distinct vibrations by IR spectroscopy.

A single water molecule can be surgically inserted into a C_{60} cage in a process pioneered by Kurotobi and Murata.[9] Due to the polarity of the water molecule, $H_2O@C_{60}$ is of interest in the context of making water-soluble and biocompatible fullerenes.[27] Surprisingly, it was subsequently found that the dipole moment is significantly shielded, reduced to 0.51 ± 0.05 D from 1.85 D for free water.[28,29] This has been explained by an electrostatic response of the cage, where the π-electrons inside the cage become polarised, shifting in a way that mirrors the dipole moment of the water molecule.[30] A similar screening effect and reduction in dipole moment has been seen for $HF@C_{60}$.[8,31] A consequence of this effect is that the IR intensities of the vibrational modes of the encapsulated water are reduced relative to those of free water in condensed-phase studies.[9,29] The H_2O features are also slightly red-shifted due to attractive interactions with the cage.[29,32] Interestingly, the cage vibrational modes are relatively unperturbed,[9,29] indicating that the water molecule does not have much influence on the geometric structure of the cage. Furthermore, the electronic spectrum of $H_2O@C_{60}$ in solution has been recorded and there is little difference from that of C_{60}.[9] This implies that the frontier molecular orbitals are unperturbed by the presence of the water molecule.[33] It should be noted, however, that $H_2O@C_{60}$ has no narrow electronic features for comparison to DIBs and small perturbations will be hard to observe for the broader UV/Vis features.

The charged species, $H_2O@C_{60}^+$, has also been studied previously. The electronic spectrum, recorded by messenger tagging spectroscopy, looks considerably different to that of C_{60}^+ due to cage transitions being accompanied by rotational excitation of the water molecule.[34] Here, mid-IR spectra are presented for $H_2O@C_{60}^+$ and $H_2O@C_{60}H^+$ in the gas phase. These are compared to the spectra of the respective empty fullerenes to probe the influence of the encapsulated water molecule on the spectroscopic properties in the IR. The results are discussed in the context of the detectability of endohedral fullerenes with encapsulated polar molecules in astrophysical environments through IR spectroscopy.

2 Methods

2.1 IRMPD spectroscopy of $H_2O@C_{60}H^+$

The infrared multiple photon dissociation (IRMPD) spectra of $C_{60}H^+$ and $H_2O@C_{60}H^+$ ions were measured in a 3-D quadrupole ion trap (QIT, Bruker amaZon speed ETD) that has been modified to be coupled to FELIX, the Free-Electron Laser for Infrared eXperiments.[35,36]

Ions were produced in an atmospheric pressure chemical ionization (APCI, Bruker APCI II) source using a direct insertion probe (DIP, Bruker DP) inlet that has been used previously to ionize apolar substances like PAHs[37] and fullerenes.[38,39] The APCI-DIP source consumes a minimal amount of sample, which is especially practical when using precious materials, such as endohedral fullerenes. A sample of C_{60} (MER Corporation, USA) or $H_2O@C_{60}$, synthesised using a 'molecular surgery' approach,[9,10] was placed on the glass capillary and introduced to the ion source. The settings of the APCI-DIP source were optimised for the production of fullerene ions.[40]

Due to the natural abundance of ^{13}C, the mass spectrum (Fig. S1 in the SI) will be a superposition of the radical cation and the protonated ion of the species. To record a vibrational spectrum, $C_{60}H^+$ (*m*/*z* 721) or $H_2O@C_{60}H^+$ (*m*/*z* 739) ions were isolated and irradiated with tunable laser light. The loss of a hydrogen atom resulted in new peaks appearing in the mass spectra at *m*/*z* 720 or *m*/*z* 738, indicating the presence of C_{60}^+ or $H_2O@C_{60}^+$, respectively. This fragmentation behaviour allows the measurement of the IR spectra of the protonated ions independent of the overlapping presence of the ^{13}C radical cations. The mass spectrum of the ions in the trap was recorded following exposure to the tunable laser light. The frequency was tuned in steps of 4 cm^{-1} and the measurement repeated. The wavelength-dependent fragmentation yield was calculated by:

$$Y(\lambda) = \frac{I_{\text{fragment}}}{(1-x)\cdot[I_{\text{fragment}} + I_{\text{parent}}]} \quad (1)$$

where *x* is the fraction of the peak intensity contributed by the ^{13}C radical cation at the relevant *m*/*z*. This was 0.16 for $H_2O@C_{60}H^+$ and 0.13 for $C_{60}H^+$. The spectra were plotted in terms of the fragment fluence, *S*, which is proportional to the absorption cross-section, using:[41]

$$S(\lambda) = -\ln(1 - Y) \quad (2)$$

$S(\lambda)$ was then corrected for the laser pulse energy and irradiation time.

In the 3 μm region, the helium buffer gas pressure in the quadrupole ion trap was reduced to a minimum. This allowed the detection of lower intensity peaks in the spectrum by reducing the collisional quenching of the IR-excited ions.[39]

FELIX produces 7 μs macropulses at a 10 Hz repetition rate that consist of a train of micropulses spaced by 1 ns. The micropulses are Fourier-transform limited and have a bandwidth of 0.4% of the IR frequency. The IR spectrum was recorded between 3 and 10 μm. In this wavelength region, FELIX produces macropulse energies up to approximately 150 mJ. The wavelength was calibrated using a grating spectrometer with an accuracy of ±0.01 μm.

2.2 Messenger tagging spectroscopy of $H_2O@C_{60}^+$

The IR absorption spectrum of the endohedral fullerene, $H_2O@C_{60}^+$, was measured by helium tagging spectroscopy, using a combination of ion spectroscopy and mass spectrometry. The cryogenic ion-trapping apparatus has previously been described in detail[42] and only further details specific to the present work are given here.

The $H_2O@C_{60}$ sample was vaporised in an oven heated to ~350 °C. Singly charged cations were generated from 50 eV electron impact ionisation of the neutral sample before being injected into a linear quadrupole ion trap. Within the trap, the ions were internally cooled by collisions with dense helium buffer gas (10^{15} cm^{-3}) in equilibrium with the trap walls (T_{nom} = 4.7 K). The flexible timescale afforded by the trap allowed for the formation of weakly bound ion-helium complexes (Fig. S2 in the SI). The helium tag has a low binding energy of ~100 cm^{-1},[43,44] meaning that the complex readily dissociates following one photon excitation. In the spectroscopic investigation, the depletion of $H_2O@C_{60}^+$–He complexes (m/z 742) was monitored as a function of wavelength, providing a sensitive proxy for absorption.

A Nd:YAG (Amplitude Laser Inc.) pumped OPO/OPA (LaserVision) was used as the source of radiation, operating with a repetition rate of 10 Hz and a linewidth of 0.9 cm^{-1}. Mid-IR radiation was generated (~0.2 mJ per pulse) by difference frequency generation using a $AgGaSe_2$ crystal and focused into the ion trap using a ZnSe lens (f = 25 cm). The ion cloud was exposed to four pulses of radiation per trapping cycle (1 Hz). A mechanical shutter was used to control exposure to radiation so that the number of helium-tagged complexes could be measured with (N_i) and without (N_0) irradiation on alternate trapping cycles. The presented spectra were corrected for variations in relative OPO/OPA fluence, ϕ, with wavelength and plotted in terms of the relative cross-section using:

$$\sigma_{rel} = -\frac{\ln(N_i/N_0)}{\phi} \quad (3)$$

The spectra were individually normalised so that the most intense absorption features have σ_{rel} = 1. The wavelength of the near-IR output of the OPO stage was monitored to calibrate the wavelength of the mid-IR output.

2.3 Computational methods

The calculations presented for all species in this work were carried out at the DFT level of theory using Orca 6.0.1.[45–50] The B3LYP/cc-pVDZ functional and basis set[51] were employed for the geometry optimisation and frequency calculations, with a D4 empirical dispersion correction[52–55] applied to account for long-range dispersion interactions. To best simulate the experimental profiles, the calculated vibrational transitions of $C_{60}H^+$ and $H_2O@C_{60}H^+$ were convolved using a Gaussian lineshape with an FWHM of 20 cm^{-1}, while those of C_{60}^+ and $H_2O@C_{60}^+$ were convolved using a Lorentzian lineshape with an FWHM of 10 cm^{-1}. All calculated frequencies were scaled by a factor of 0.97.[56]

The electron density change induced by the intra-complex interactions in $H_2O@C_{60}$ and $H_2O@C_{60}^+$ was calculated using $\Delta\rho^{el} = \rho^{el}_{complex} - \rho^{el}_{cage} - \rho^{el}_{water}$. Here, $\rho^{el}_{complex}$ is the electron density of the whole system, while ρ^{el}_{cage} and ρ^{el}_{water} are the electron densities of the fullerene cage and water molecule counterparts, respectively. The geometry and coordinates of the isolated fullerene and water molecule were kept the same as in the endohedral. The electron density was recorded at a number of points in a cubic grid of 12 × 12 × 12 Å^3 with a 0.1 Å interval in the x, y and z directions. The central slice of the electron density distribution is represented as a 2-D contour plot.

3 Results

3.1 $H_2O@C_{60}H^+$

Fig. 1 presents the IRMPD spectra of $C_{60}H^+$ and $H_2O@C_{60}H^+$ in the 1000–2940 cm^{-1} range, complemented with the respective theoretical spectra in the bottom panel. Strong peaks are observed in the fingerprint region between 1150 and 1600 cm^{-1} corresponding to C–C stretching modes of the fullerene cage. The weak feature at 2305 cm^{-1} has not been previously assigned, but could be caused by an overtone or combination transition observable due to the high power used. The band present at 2820 cm^{-1} arises from the C–H stretching mode. The experimental characteristics are listed in Table 1 (see Table S1 in the SI for the calculated frequencies).

Two different configurations are possible for the $H_2O@C_{60}H^+$ ions – protonation can occur on one of the carbon atoms of the fullerene[57] or on the water molecule inside the carbon cage. The molecular structure can be determined by comparing the experimental spectrum with the calculated spectrum of a known geometry (Fig. S3 in the SI). On the bottom panel of Fig. 1, the theoretical spectrum of the structure with an exohedral proton is plotted, which shows many similarities with the IRMPD spectrum and suggests the protonation site is on the carbon cage. It should be noted that the harmonically computed C–H stretch frequency is slightly too high since it requires a frequency scaling factor that is distinct from that of the bands at lower wavelengths.[39]

Comparing the spectrum of $H_2O@C_{60}H^+$ to that of $C_{60}H^+$ reveals that the two vibrational spectra are almost completely identical. This indicates that the encapsulated water molecule has little influence on the structure and vibrations of the cage because the observed features correspond to equivalent vibrational modes of $C_{60}H^+$. There is a slight shift between the peaks that is not consistent throughout the spectrum. The $H_2O@C_{60}H^+$

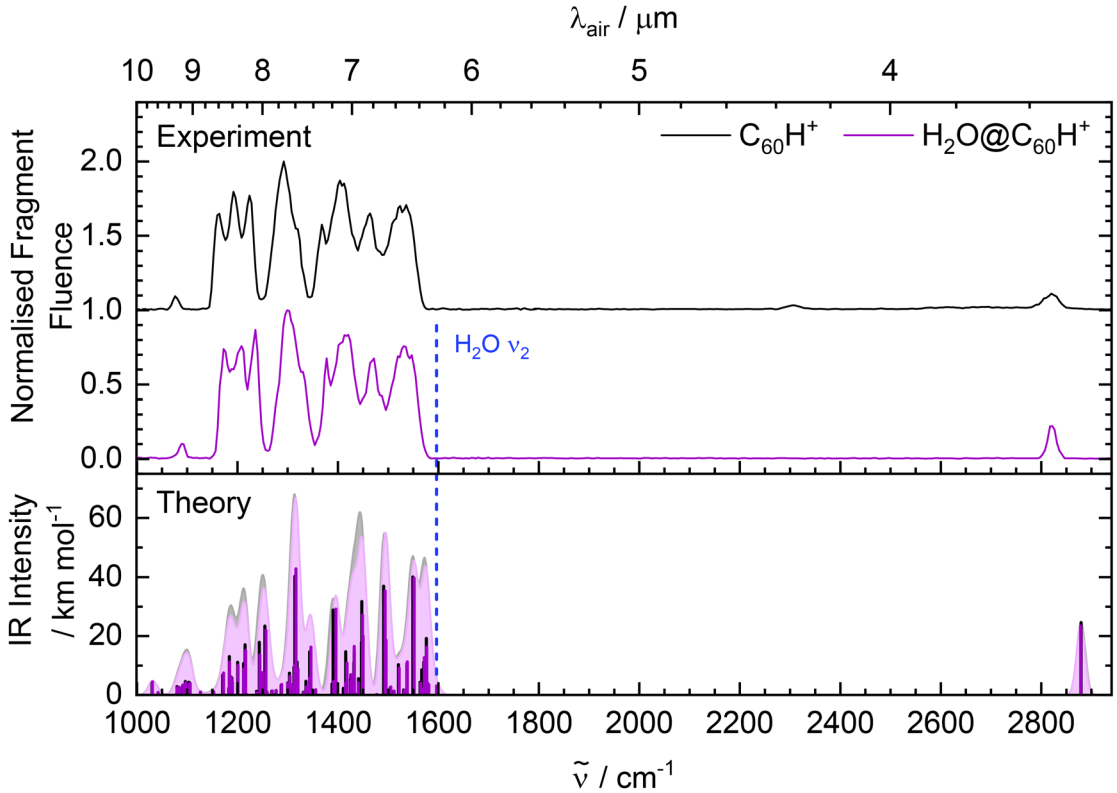

Fig. 1 IRMPD spectra of $C_{60}H^+$ (black) and $H_2O@C_{60}H^+$ (purple) complemented with DFT calculations at the B3LYP/cc-pVDZ level of theory. The $C_{60}H^+$ spectrum is offset vertically for clarity. The calculated frequency of the H_2O bending mode in $H_2O@C_{60}H^+$ is indicated by the blue dashed line at 1596.4 cm^{-1}.

Table 1 A comparison of the experimental spectra of $C_{60}H^+$ and $H_2O@C_{60}H^+$, where $\tilde{\nu}$ are the band maxima. Δ are the blue-shift in cm^{-1} of the $H_2O@C_{60}H^+$ band maxima relative to the spectrum of $C_{60}H^+$

$C_{60}H^+$		$H_2O@C_{60}H^+$		
$\tilde{\nu}$/cm^{-1}	Normalised fragment fluence	$\tilde{\nu}$/cm^{-1}	Normalised fragment fluence	Δ/cm^{-1}
1076	0.09	1089	0.10	13
1164	0.65	1173	0.74	9
1192	0.80	1208	0.76	16
1224	0.77	1236	0.87	12
1292	1	1299	1	7
1368	0.58	1378	0.68	10
1404	0.87	1421	0.83	17
1464	0.65	1472	0.68	8
1516	0.62	1519	0.69	3
1524	0.70	1531	0.76	7
1536	0.71	1547	0.70	11
2305	0.03	—[a]	—	—
2820	0.11	2822	0.22	2

[a] Feature is not present in this spectrum. However, a weak feature at ~2320 cm^{-1} could be observed when a higher power was used.

bands in the fingerprint region are blue-shifted by ~3–17 cm^{-1} relative to those of $C_{60}H^+$, while the band corresponding to the C–H stretching mode is blue-shifted by only ~2 cm^{-1}. This blue-shift is most likely due to repulsive interactions with the extra electron density from the water molecule, resulting in a 'stiffer' vibrational motion of the cage. IR spectra of noble gas endohedral fullerenes also show shifted cage features, attributed to interactions between the encapsulated atom and the carbon cage.[58,59]

Surprisingly, there are no traces of vibrations from the water molecule in the measured spectrum of $H_2O@C_{60}H^+$. The water bending mode has been measured at ~1570 cm^{-1} for solid $H_2O@C_{60}$,[29,32] which is both red-shifted and weaker in intensity than that of free water at 1595 cm^{-1}.[60] The bending mode is predicted in the theoretical spectrum of $H_2O@C_{60}H^+$ at 1596 cm^{-1}, although with an IR intensity only of 3.07 km mol^{-1}. After close inspection of the experimental spectra in this region, it appears that the features of both $C_{60}H^+$ and $H_2O@C_{60}H^+$ have very similar profiles with no clear additional contribution from the water bending mode. Possible reasons for the calculated reduction in IR intensity will be discussed in detail in Section 3.2. The IRMPD spectrum of $H_2O@C_{60}H^+$ was also measured up to 3770 cm^{-1} (Fig. S4 in the SI) in search of the water stretching modes. These are at 3657 cm^{-1} and 3756 cm^{-1} for free water,[60] but expected to be red-shifted by around 90 cm^{-1} in the endohedral fullerene.[29,32] This is towards the end of the wavelength range of FELIX so the power dropped significantly. However, the experiment was specifically optimised to observe weaker peaks and even with these conditions, no extra features can be seen beyond the C–H stretch.

Due to the nature of the IRMPD process, possible experimental limitations must be considered. During multiphoton dissociation, photon absorption at a vibrational frequency is distributed among the other vibrations of the molecule *via* intramolecular vibrational redistribution (IVR).[61] This leads to

an increase in internal energy until it reaches the threshold for dissociation of the molecule. For the water vibrational modes to be observable in the measured spectrum, the water molecule must be coupled to the C–H stretching mode, so that excitation results in the loss of the hydrogen atom. Therefore, it is not currently clear if the lack of water vibrational modes is due to an experimental limitation or caused by some other effect. To further investigate, the spectrum of the equivalent $H_2O@C_{60}^+$ was recorded by messenger tagging spectroscopy. This technique relies on the loss of a weakly bound helium tag, instead of the fragmentation of a C–H bond, so provides a more sensitive method to explore the cause of the missing water vibrational modes.

3.2 $H_2O@C_{60}^+$

The photofragmentation spectra of C_{60}^+–He and $H_2O@C_{60}^+$–He, along with the respective theoretical spectra, are presented in Fig. 2 for the 1150–1685 cm^{-1} region. The experimental characteristics are compared in Table 2. The spectrum of C_{60}^+ was recorded by Douglas-Walker *et al.*[62] using the same method and apparatus as for $H_2O@C_{60}^+$.

It is important to note that the helium tag might have some influence on the band maxima of the spectral features observed. For C_{60}^+, it has been shown that the attachment of the helium tag results in a small blue-shift of less than 1 cm^{-1}.[62] A similar perturbation is expected for the spectrum of $H_2O@C_{60}^+$. The position of the band maxima can, therefore, be approximated to those of the untagged ion. The width of the spectral features (of the order of $\sim$10 cm^{-1}) is likely to be caused by the short lifetime of the excited ion-helium complex as discussed by Douglas-Walker *et al.*[62]

The experimental $H_2O@C_{60}^+$ spectrum shows a prominent band at 1408 cm^{-1} with three weaker features at approximately 1232, 1343 and 1560 cm^{-1}. Upon examination of Fig. 2, it is clear that the spectrum is remarkably similar to that of C_{60}^+ with many of the same features present. A closer inspection of Table 2 reveals that that the band maxima of the features of $H_2O@C_{60}^+$ are blue-shifted by $\sim$6–18 cm^{-1} relative to the spectrum of C_{60}^+. This is consistent with what was observed for the vibrational spectrum of the protonated equivalent. As discussed previously, these observations imply that the water molecule only has a small influence on the geometric structure of the cage with the blue-shift caused by some minor repulsive interactions.

For both $H_2O@C_{60}^+$ and C_{60}^+, some of the features show structure suggestive of the contribution of additional unresolved bands. This phenomenon has already been documented for C_{60}^+ and attributed to either a distortion in geometry from D_{5d} or anharmonic effects.[62] The calculations presented here (Table S2 in the SI) predict a greater loss in degeneracy for $H_2O@C_{60}^+$ than for C_{60}^+, suggesting that the presence of H_2O causes a larger reduction in symmetry of the C_{60}^+ cage. There is some indication of this in the experimental spectra, where the asymmetry of the

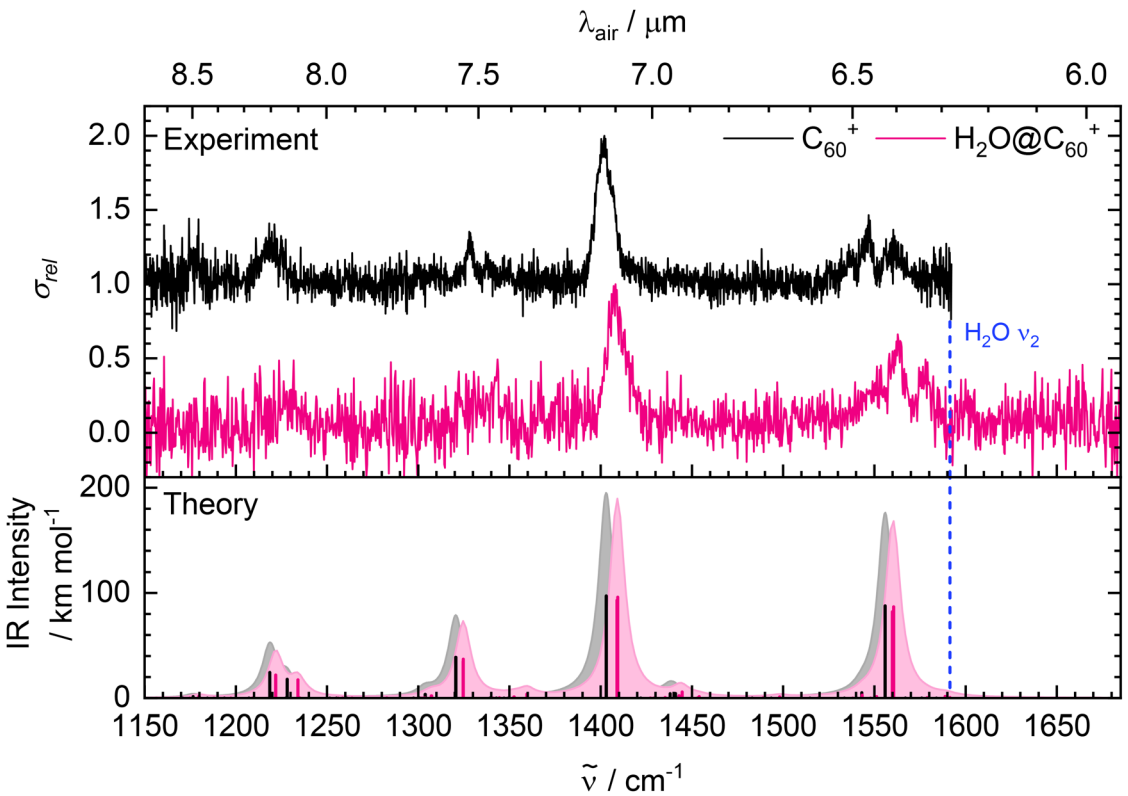

Fig. 2 Photofragmentation spectra of C_{60}^+–He (black) and $H_2O@C_{60}^+$–He (pink) complemented with DFT calculations at the B3LYP/cc-pVDZ level of theory. The C_{60}^+ spectrum is offset vertically for clarity. The calculated frequency of the H_2O bending mode in $H_2O@C_{60}^+$ is indicated by the blue dashed line at 1591.4 cm^{-1}.

Table 2 A comparison of the experimental spectra of C_{60}^+–He and $H_2O@C_{60}^+$–He. $\tilde{\nu}$ are the band maxima and are reported with an error of ±1 cm^{-1}. Δ are the blue-shift in cm^{-1} of the $H_2O@C_{60}^+$–He band maxima relative to the spectrum of C_{60}^+–He

C_{60}^+–He			$H_2O@C_{60}^+$–He		
Symmetry	$\tilde{\nu}$/cm^{-1}	σ_{rel}	$\tilde{\nu}$/cm^{-1}	σ_{rel}	Δ/cm^{-1}
E_{1u}/A_{2u}	1179	0.44	—	—	—
E_{1u}/A_{2u}	1218	0.41	1232	0.49	14
E_{1u}	1328	0.35	1343	0.49	15
E_{1u}	1402	1	1408	1	6
	1536	0.27	1554	0.45	18
E_{1u}	1547	0.46	1563	0.66	16
	1560	0.37	1578	0.49	18

feature at ~1400 cm^{-1} appears to be more pronounced for the endohedral fullerene. While some loss in degeneracy is evident, it is remarkable how little influence encapsulating a water molecule has on the geometric structure of the cage. The structure of the feature at ~1550 cm^{-1} is not predicted by the harmonic vibrational frequency calculations and is most likely due to anharmonic effects, such as combination bands.

Interestingly, the water bending mode is not seen in the spectrum of $H_2O@C_{60}^+$, as also observed for $H_2O@C_{60}H^+$. In the case of $H_2O@C_{60}H^+$ measured by IRMPD, there was some uncertainty on whether this was caused by an experimental limitation due to the energy required to break the C–H bond. The helium tag has a much lower binding energy of ~100 cm^{-1} so a vibrational energy of ~1600 cm^{-1} should be sufficient to cause dissociation.[43,44] Another consideration is the timescale for dissociation of the ion-helium complex. Excitation of the C_{60}^+ cage vibrations give absorptions with FWHMs of around 10 cm^{-1} or less, implying picosecond lifetimes of the C_{60}^+–He complex. However, if the encapsulated water molecule is only weakly coupled to the cage, there is a possibility that the redistribution of vibrational energy from excited H_2O modes to the cage is so slow that the loss of the helium tag does not occur before the ions are detected. In the present experiment, a delay of approximately 50 ms between the last laser pulse and the end of the trapping cycle was used, which is believed to be ample time to observe the loss of the helium tag. Furthermore, a previous study on the electronic spectrum of $H_2O@C_{60}^+$ recorded using the same technique and apparatus may support this assumption.[34] In that study, only bands associated with the lowest H_2O rotational states were observed indicating that the encapsulated H_2O had been cooled, presumably through collisions between helium and the C_{60}^+ cage within the experimental timescale. Given that little is known about how vibrational redistribution occurs in endohedral fullerenes, it could form the topic of an interesting theoretical study. In any case, a direct spectroscopy technique would be required to experimentally confirm whether the lack of observed H_2O vibrational modes is an experimental limitation.

Theory also predicts quite a drastic reduction in the IR intensity of the water bending mode upon the encapsulation of H_2O, implying that there might be some other effect occurring. The intensities are calculated as 0.6 km mol^{-1} (at 1591 cm^{-1}) for $H_2O@C_{60}^+$ compared to 55.62 km mol^{-1} (at 1608 cm^{-1}) for an isolated water molecule. As described in Section 1, a reduction in IR intensity has been observed experimentally for the water bending mode of $H_2O@C_{60}$ in the condensed phase.[29] This has been justified by a shielding effect of the cage, where the π-electrons polarise in a way that mirrors the dipole of the internal water.[30,63] A similar effect is, therefore, expected to be at play in $H_2O@C_{60}^+$.

Fig. 3 presents the change in electron density induced in $H_2O@C_{60}^+$ and $H_2O@C_{60}$ relative to the isolated water and fullerene counterparts. For both species, it is clear that the electron density of the cage shields the dipole of the water molecule and that it is primarily the electrons inside the cage that are affected. This single-sided response is consistent with the idea that C_{60} acts as a Faraday cage, shielding ~75% of applied electric fields.[30,64] From these contour plots, it appears that C_{60}^+ also acts as a Faraday cage, shielding the electrons outside the cage from the influence of the water molecule. Importantly, the cage appears to be polarised to a greater extent for $H_2O@C_{60}^+$, indicating that there are stronger intermolecular

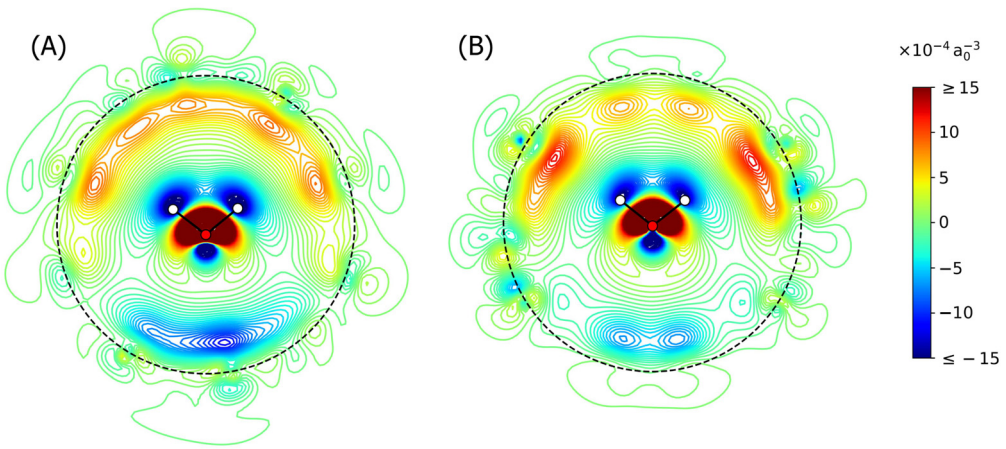

Fig. 3 Contour plots of the electron density change induced in (A) $H_2O@C_{60}^+$ and (B) $H_2O@C_{60}$, calculated using $\Delta\rho^{el} = \rho^{el}_{complex} - \rho^{el}_{cage} - \rho^{el}_{water}$. The central slice of the distribution has been plotted.

interactions between the open-shell cage and the water molecule. Dipole moments are calculated as 0.31 D for $H_2O@C_{60}$ and 0.07 D for $H_2O@C_{60}^+$ (compared to 1.94 D calculated for H_2O) further supporting the hypothesis of a stronger shielding effect for the charged system. It should be noted that the dipole moment for $H_2O@C_{60}$ has been documented to be closer to $\sim$0.5 D,[28,29,63] but it is believed that the chosen level of theory in the present work provides a valid qualitative comparison between the different species with all of the essential physics modelled.

To link this to IR intensity, the dipole derivative must be considered. A polarisable cage would allow the inner π-electrons to rapidly rearrange as the water molecule moves through its vibrational mode (Fig. S5 in the SI), reducing the dipole moment at each stage of the motion. This results in an overall reduction in the change of dipole moment during the vibrational mode and hence the IR intensity. If the cage is more polarisable, as expected for $H_2O@C_{60}^+$, the electrons will be more mobile and the IR intensity will be reduced even further. For $H_2O@C_{60}$, theory predicts an IR intensity of 2.38 km mol^{-1} (at 1588.3 cm^{-1}) for the water bending mode, which is 2.9% of the intensity of the most intense cage transition. In comparison, the calculated bending mode for $H_2O@C_{60}^+$ has a relative IR intensity of 0.3%, which would likely be too weak to be observed in these experiments. The polarisation effect is expected to be the dominant factor in the reduction of the IR intensities[30] so this offers an explanation as to why the water bending mode is not observed in the experimental spectrum of $H_2O@C_{60}^+$. The region where the water stretching modes should appear was not measured experimentally here, but the calculations also predict that they are reduced in intensity (Table S3 in the SI) presumably due to the same effect.

4 Astrochemical implications

Although the role of endohedral fullerenes in interstellar chemistry is yet to be uncovered, they have been proposed to be responsible for the presence of ^{22}Ne in ancient meteorites.[23] ^{22}Ne is thought to be formed from the decay of ^{22}Na following a supernova explosion, which is rapidly trapped during carbon condensation. The entrapment of ^{22}Na within C_{60} has been shown as rapid and selective in conditions simulating stellar environments and so has been proposed as the dominant mechanism for the enrichment of meteorites.[23] Furthermore, extraterrestrial fullerenes containing noble gases have been reported in meteorites and sediment samples,[65] although the analysis method had been found capable of false positive signals.[66] The survivability of these endohedral fullerenes through impact events might indicate that this is a feasible pathway for the delivery of organic species to Earth.[65] Endohedral fullerenes have yet to be detected in space, but it is clear that their detection would have important implications for interstellar chemistry or even astrobiology.

The formation of endohedral fullerenes in space is not fully understood so it is difficult to predict which specific species will be abundant. However, water is a useful molecule for spectroscopic characterisation because it has a dipole moment and relatively strong IR transitions. In theory, this means that it is a good example to investigate how the encapsulated molecule vibrates inside the cage. Surprisingly, no water vibrational modes were observed in the spectra of either $H_2O@C_{60}H^+$ or $H_2O@C_{60}^+$ in the gas phase. The lack of detection is assumed to be caused by a shielding effect of the cage rather than an experimental artefact of the technique used, although the latter explanation cannot be completely discounted (see Section 3.2). While it was expected for the cage transitions to be perturbed by the water molecule, the IR spectra of both $H_2O@C_{60}H^+$ and $H_2O@C_{60}^+$ look remarkably similar to those of the empty fullerenes, with the features only slightly blue-shifted. This indicates that the internal water molecule has little influence on the geometric structure and vibrations of the cage. The astronomical implications of these results are significant, as discussed in detail below.

The experimental spectra presented here are representative of absorption spectra, whereas astronomical observations are of IR emission. This is thought to arise due to cascade emission from UV-pumped molecules, which often leads to broader features compared to absorption.[14,67] For a C_{60} analogue to be clearly distinguishable by its IR emission spectrum, the perturbation of the cage vibrations must be quite large compared to the widths. In the case of $H_2O@C_{60}H^+$ and $H_2O@C_{60}^+$, the blue-shift of the features relative to the empty cage is small, which means that the features will overlap. It is reasonable to assume that the endohedral fullerene will have some fraction of the cosmic abundance of the empty fullerene, hence astronomical spectra will be dominated by features of the empty cage (Fig. S6 in the SI). Consequently, astronomical detection of $H_2O@C_{60}H^+$ and $H_2O@C_{60}^+$ by IR emission in the region containing the cage vibrations would be extremely challenging. While no H_2O vibrational modes were seen in these experiments, and theory predicts a shielding effect that gives rise to a significant reduction in IR intensity, it cannot be completely ruled out that weak H_2O modes may be detectable by IR emission.

It is expected that this line of reasoning can be extended to other endohedral fullerenes. A multitude of endohedral fullerenes have been studied experimentally or theoretically and appear to exhibit the same vibrational features as the empty cage, including $H_2@C_{60}^+$,[26] $CH_4@C_{60}$,[68] $H_2O@C_{60}$,[9] $Ar@C_{60}$,[58] $Kr@C_{60}$,[58] $SnH_4@C_{60}$[69] and $N_2@C_{60}$.[70] Vibrational spectra have been calculated for a variety of endohedral metallofullerenes; these also show overlapping features with the empty cage along with many extra features.[24] Although the extent of the interactions are dependent on both the type of guest species and the cage, the examples here imply that light molecules inside carbon cages behave in similar ways. This indicates that it will generally be difficult to distinguish between endohedral fullerenes and their empty cage based on the cage vibrational modes.

There are other viable routes to identify endohedral fullerenes in space, including rotational or electronic spectroscopy. The intensity of rotational transitions is dependent on the dipole moment so it is difficult to detect empty fullerenes using

this method. Encapsulating a polar molecule results in a net dipole moment, but the shielding effect of the cage means that the rotational transitions will not necessarily be strong enough for astronomical detection. However, the detection of molecules by rotational spectroscopy is continuously developing, allowing the astronomical detection of indene with a dipole moment only of $\sim$0.73 D[71] and, more recently, of cyanocoronene,[72] which is the largest non-fullerene molecule to be detected in space. Therefore, it is not inconceivable that polar fullerene derivatives will be rotationally detectable in the future.

Electronic spectroscopy for comparison with DIBs could also be feasible to identify endohedral fullerenes in space. This would require that the electronic structure is perturbed enough by the encapsulated molecule so that the features can be resolved. For $H_2O@C_{60}^+$, electronic transitions are coupled with water rotational modes, resulting in a spectrum that looks considerably different than the empty cage.[34] The electronic spectrum of $H_2@C_{60}^+$ is also distinguishable from C_{60}^+,[26] the formation of which might be more favourable in space due to the high abundance of H_2 in the interstellar medium.[73] While these examples show that electronic spectra can differ for the endohedral fullerene, detection by electronic spectroscopy comes with its own challenges. The DIBs assigned to C_{60}^+ are relatively weak absorptions and in a region strongly contaminated by telluric water absorptions.[74] Any endohedral fullerene will likely be less abundant than C_{60}^+, so would be very hard to detect in the vicinity of the C_{60}^+ transitions using ground-based telescopes. However, more studies are required to understand how electronic spectra vary for different types of endohedral fullerenes and what interactions lead to greater perturbations of the electronic structure.

5 Conclusions

Gas-phase mid-IR spectra have been presented for $H_2O@C_{60}^+$ and $H_2O@C_{60}H^+$, obtained using action spectroscopy techniques. These are the first gas-phase IR spectra of an endohedral fullerene with an IR-active guest. The spectra bear a close resemblance to those of the equivalent empty fullerenes, implying only a small perturbation to the geometric structure of the cage upon the encapsulation of H_2O. The band maxima are slightly blue-shifted, suggestive of some repulsive interactions. The water bending mode could not be observed in either of the measured spectra with theory predicting a polarisation of the π-electrons of the cage, reducing the dipole moment and IR intensity. Although these experiments failed to detect the IR absorption of the water vibrational modes, one cannot exclude the possibility that weak modes could be present in IR emission, relevant to astronomical observations. However, it will be difficult to distinguish between the endohedral and empty fullerene using IR spectroscopy in the vicinity of the cage modes. As a result, astronomical detection by IR emission will be challenging and other spectroscopic techniques should be considered. More studies are required on electronic or rotational spectroscopy to understand the interactions that lead to distinguishable spectra. $H_2O@C_{60}^+$ and $H_2O@C_{60}H^+$ were chosen as a proxy to try and understand the general behaviour of endohedrals with polar guests, so it is expected that this line of reasoning can be extended to other endohedral fullerenes.

Author contributions

O. O'Neill: formal analysis (lead), investigation (equal), visualisation (lead), writing – original draft (lead), writing – review and editing (equal); J. Palotás: formal analysis (supporting), investigation (equal), writing – original draft (supporting), writing – review and editing (equal); T. E. Douglas-Walker: investigation (equal), writing – review and editing (equal); R. J. Whitby: resources (lead), writing – review and editing (equal); M. H. Levitt: writing – review and editing (equal); G. R. Bacanu: writing – review and editing (equal); C. S. Anstöter: supervision (supporting), writing – review and editing (equal); G. Berden: investigation (equal), writing – review and editing (equal); J. Oomens: supervision (supporting), writing – review and editing (equal); E. K. Campbell: funding acquisition (lead), supervision (lead), writing – review and editing (equal).

Conflicts of interest

There are no conflicts to declare.

Data availability

The data supporting this article are included within the submitted manuscript. Raw data used to plot the figures are available from the corresponding authors upon reasonable request.

Supplementary information (SI): calculations for H_2O, C_{60}^+, $C_{60}H^+$, $H_2O@C_{60}^+$, $H_2O@C_{60}H^+$ and $H_3O^+@C_{60}$; experimental mass spectra; IRMPD spectrum of $H_2O@C_{60}H^+$ up to 3770 cm^{-1}; and photofragmentation spectrum of a mixture of C_{60}^+–He and $H_2O@C_{60}^+$–He. See DOI: https://doi.org/10.1039/d6cp00593d.

Acknowledgements

The authors acknowledge the financial assistance from the Royal Society (grant numbers RGF/EA/181035, RF/ERE/210238, URF/R1/180162, and URF/R/231018) and Engineering and Physical Sciences Research Council (grant numbers EP/W03753X/1 and EP/T004320/1). This research work has been funded in memory of Dr Brian R Phillips, 1958 and 1961 graduate of the University of Edinburgh. This article is based upon work from COST Action CA21126–Carbon molecular nanostructures in space (NanoSpace), supported by COST (European Cooperation in Science and Technology). Calculations on the protonated system were performed at the SurfSARA Supercomputer centre

with compute budget kindly provided through NWO Rekentijd grant 2024.009.

References

1 H. W. Kroto, J. R. Heath, S. C. O'Brien, R. F. Curl and R. E. Smalley, *Nature*, 1985, **318**, 162–163.
2 J. R. Heath, S. C. O'Brien, Q. Zhang, Y. Liu, R. F. Curl, F. K. Tittel and R. E. Smalley, *J. Am. Chem. Soc.*, 1985, **107**, 7779–7780.
3 T. Weiske, D. K. Böhme, J. Hrušák, W. Krätschmer and H. Schwarz, *Angew. Chem., Int. Ed. Engl.*, 1991, **30**, 884–886.
4 J. C. Hummelen, M. Prato and F. Wudl, *J. Am. Chem. Soc.*, 1995, **117**, 7003–7004.
5 Y. Rubin, *Chem. – Eur. J.*, 1997, **3**, 1009–1016.
6 S. Bloodworth and R. J. Whitby, *Commun. Chem.*, 2022, **5**, 121.
7 K. Komatsu, M. Murata and Y. Murata, *Science*, 2005, **307**, 238–240.
8 A. Krachmalnicoff, R. Bounds, S. Mamone, S. Alom, M. Concistrè, B. Meier, K. Kouřil, M. E. Light, M. R. Johnson, S. Rols, A. J. Horsewill, A. Shugai, U. Nagel, T. Rõõm, M. Carravetta, M. H. Levitt and R. J. Whitby, *Nat. Chem.*, 2016, **8**, 953–957.
9 K. Kurotobi and Y. Murata, *Science*, 2011, **333**, 613–616.
10 A. Krachmalnicoff, M. H. Levitt and R. J. Whitby, *Chem. Commun.*, 2014, **50**, 13037–13040.
11 S. Bloodworth, G. Sitinova, S. Alom, S. Vidal, G. R. Bacanu, S. J. Elliott, M. E. Light, J. M. Herniman, G. J. Langley, M. H. Levitt and R. J. Whitby, *Angew. Chem., Int. Ed.*, 2019, **58**, 5038–5043.
12 F. Cataldo, G. Strazzulla and S. Iglesias-Groth, *Mon. Not. R. Astron. Soc.*, 2009, **394**, 615–623.
13 R. D. Beck, P. Weis, J. Rockenberger and M. M. Kappes, *Surf. Rev. Lett.*, 1996, **03**, 771–775.
14 K. Sellgren, M. W. Werner, J. G. Ingalls, J. D. T. Smith, T. M. Carleton and C. Joblin, *Astrophys. J., Lett.*, 2010, **722**, L54–L57.
15 J. Cami, J. Bernard-Salas, E. Peeters and S. E. Malek, *Science*, 2010, **329**, 1180–1182.
16 Y. Zhang and S. Kwok, *Astrophys. J.*, 2011, **730**, 126.
17 S. Iglesias-Groth and M. Esposito, *Astrophys. J., Lett.*, 2013, **776**, L2.
18 E. K. Campbell, M. Holz, D. Gerlich and J. P. Maier, *Nature*, 2015, **523**, 322–323.
19 B. H. Foing and P. Ehrenfreund, *Nature*, 1994, **369**, 296–298.
20 J. Fulara, M. Jakobi and J. P. Maier, *Chem. Phys. Lett.*, 1993, **211**, 227–234.
21 M. Šala, M. Hodošček, S. Arulmozhiraja and T. Fujii, *J. Phys. Chem. A*, 2009, **113**, 3223–3226.
22 H. W. Kroto and M. Jura, *Astron. Astrophys.*, 1992, **263**, 275–280.
23 P. W. Dunk, J.-J. Adjizian, N. K. Kaiser, J. P. Quinn, G. T. Blakney, C. P. Ewels, A. G. Marshall and H. W. Kroto, *Proc. Natl. Acad. Sci. U. S. A.*, 2013, **110**, 18081–18086.
24 R. Barzaga, D. A. García-Hernández, S. Díaz-Tendero, S. Sadjadi, A. Manchado and M. Alcami, *Astrophys. J.*, 2023, **942**, 5.
25 G. R. Bacanu, *Chem. Phys. Rev.*, 2025, **6**, 031307.
26 D. V. Strelnikov, J. Jašík, D. Gerlich, M. Murata, Y. Murata, K. Komatsu and J. Roithová, *J. Phys. Chem. A*, 2018, **122**, 8162–8166.
27 A. L. Balch, *Science*, 2011, **333**, 531–532.
28 B. Meier, S. Mamone, M. Concistrè, J. Alonso-Valdesueiro, A. Krachmalnicoff, R. J. Whitby and M. H. Levitt, *Nat. Commun.*, 2015, **6**, 8112.
29 A. Shugai, U. Nagel, Y. Murata, Y. Li, S. Mamone, A. Krachmalnicoff, S. Alom, R. J. Whitby, M. H. Levitt and T. Rõõm, *J. Chem. Phys.*, 2021, **154**, 124311.
30 H. Torii, S. Sadai, Y. Hashikawa, Y. Murata and Y. Ikemoto, *J. Phys. Chem. A*, 2024, **128**, 10867–10874.
31 P. L. Silvestrelli, S. Subashchandrabose, A. Seif and A. Ambrosetti, *Carbon Trends*, 2023, **10**, 100242.
32 J.-C. Chartrand, T. Putaud, G. Bélanger, M. Bertin, J.-H. Fillion, P. Léveillé, X. Michaut and P. Ayotte, *J. Chem. Phys.*, 2025, **162**, 144312.
33 S. P. Jarvis, H. Sang, F. Junqueira, O. Gordon, J. E. A. Hodgkinson, A. Saywell, P. Rahe, S. Mamone, S. Taylor, A. Sweetman, J. Leaf, D. A. Duncan, T.-L. Lee, P. K. Thakur, G. Hoffman, R. J. Whitby, M. H. Levitt, G. Held, L. Kantorovich, P. Moriarty and R. G. Jones, *Commun. Chem.*, 2021, **4**, 135.
34 J. Rademacher, E. S. Reedy, F. Negri, S. Alom, R. J. Whitby, M. H. Levitt and E. K. Campbell, *Mol. Phys.*, 2024, **122**, e2173507.
35 D. Oepts, A. F. G. van der Meer and P. W. van Amersfoort, *Infrared Phys. Technol.*, 1995, **36**, 297–308.
36 J. Martens, G. Berden, C. R. Gebhardt and J. Oomens, *Rev. Sci. Instrum.*, 2016, **87**, 103108.
37 J. Palotás, J. Martens, G. Berden and J. Oomens, *J. Mol. Spectrosc.*, 2021, **378**, 111474.
38 J. Palotás, J. Martens, G. Berden and J. Oomens, *Astrophys. J., Lett.*, 2021, **909**, L17.
39 L. Finazzi, V. J. Esposito, J. Palotás, J. Martens, E. Peeters, J. Cami, G. Berden and J. Oomens, *Astrophys. J.*, 2024, **971**, 168.
40 J. Palotás, J. Martens, G. Berden and J. Oomens, *J. Phys. Chem. A*, 2022, **126**, 2928–2935.
41 G. Berden, M. Derksen, K. J. Houthuijs, J. Martens and J. Oomens, *Int. J. Mass Spectrom.*, 2019, **443**, 1–8.
42 E. K. Campbell, M. Holz, J. P. Maier, D. Gerlich, G. A. H. Walker and D. Bohlender, *Astrophys. J.*, 2016, **822**, 17.
43 F. Calvo, *Phys. Rev. B*, 2012, **85**, 060502.
44 A. Kaiser, J. Postler, M. Ončák, M. Kuhn, M. Renzler, S. Spieler, M. Simpson, M. Gatchell, M. K. Beyer, R. Wester, F. A. Gianturco, P. Scheier, F. Calvo and E. Yurtsever, *J. Phys. Chem. Lett.*, 2018, **9**, 1237–1242.
45 F. Neese, *WIREs Comput. Mol. Sci.*, 2022, **12**, e1606.
46 F. Neese, *J. Comput. Chem.*, 2003, **24**, 1740–1747.
47 F. Neese, F. Wennmohs, A. Hansen and U. Becker, *Chem. Phys.*, 2009, **356**, 98–109.
48 D. Bykov, T. Petrenko, R. Izsák, S. Kossmann, U. Becker, E. Valeev and F. Neese, *Mol. Phys.*, 2015, **113**, 1961–1977.
49 B. Helmich-Paris, B. de Souza, F. Neese and R. Izsák, *J. Chem. Phys.*, 2021, **155**, 104109.

50 F. Neese, *J. Comput. Chem.*, 2023, **44**, 381–396.
51 T. H. Dunning, Jr., *J. Chem. Phys.*, 1989, **90**, 1007–1023.
52 E. Caldeweyher, C. Bannwarth and S. Grimme, *J. Chem. Phys.*, 2017, **147**, 034112.
53 E. Caldeweyher, S. Ehlert, A. Hansen, H. Neugebauer, S. Spicher, C. Bannwarth and S. Grimme, *J. Chem. Phys.*, 2019, **150**, 154122.
54 E. Caldeweyher, J.-M. Mewes, S. Ehlert and S. Grimme, *Phys. Chem. Chem. Phys.*, 2020, **22**, 8499–8512.
55 L. Wittmann, I. Gordiy, M. Friede, B. Helmich-Paris, S. Grimme, A. Hansen and M. Bursch, *Phys. Chem. Chem. Phys.*, 2024, **26**, 21379–21394.
56 R. D. Johnson III, *NIST Computational Chemistry Comparison and Benchmark Database, NIST Standard Reference Database Number* 101, 2022, https://cccbdb.nist.gov/.
57 J. Palotás, J. Martens, G. Berden and J. Oomens, *Nat. Astron.*, 2019, **4**, 240–245.
58 F. Cimpoesu, S. Ito, H. Shimotani, H. Takagi and N. Dragoe, *Phys. Chem. Chem. Phys.*, 2011, **13**, 9609–9615.
59 S. Brown, J. Cao, J. L. Musfeldt, N. Dragoe, F. Cimpoesu, S. Ito, H. Takagi and R. J. Cross, *Phys. Rev. B*, 2006, **73**, 125446.
60 J. Tennyson, N. F. Zobov, R. Williamson, O. L. Polyansky and P. F. Bernath, *J. Phys. Chem. Ref. Data*, 2001, **30**, 735–831.
61 N. C. Polfer, *Chem. Soc. Rev.*, 2011, **40**, 2211–2221.
62 T. E. Douglas-Walker, O. O'Neill and E. K. Campbell, *Astrophys. J.*, 2025, **992**, 175.
63 B. Ensing, F. Costanzo and P. L. Silvestrelli, *J. Phys. Chem. A*, 2012, **116**, 12184–12188.
64 P. Delaney and J. C. Greer, *Appl. Phys. Lett.*, 2004, **84**, 431–433.
65 L. Becker, R. J. Poreda and T. E. Bunch, *Proc. Natl. Acad. Sci. U. S. A.*, 2000, **97**, 2979–2983.
66 M. R. Hammond and R. N. Zare, *Geochim. Cosmochim. Acta*, 2008, **72**, 5521–5529.
67 C. J. Mackie, A. Candian, T. J. Lee and A. G. G. M. Tielens, *Theor. Chem. Acc.*, 2021, **140**, 124.
68 A. Jaworski and N. Hedin, *Phys. Chem. Chem. Phys.*, 2021, **23**, 21554–21567.
69 Y. Zhang, S. Peng, X. J. Li and D. X. Zhang, *J. Mol. Struct. THEOCHEM*, 2009, **906**, 41–45.
70 Z. Slanina, F. Uhlík, T. Akasaka, X. Lu and L. Adamowicz, *Nanomaterials*, 2025, **15**, 1287.
71 A. M. Burkhardt, K. Long Kelvin Lee, P. B. Changala, C. N. Shingledecker, I. R. Cooke, R. A. Loomis, H. Wei, S. B. Charnley, E. Herbst, M. C. McCarthy and B. A. McGuire, *Astrophys. J., Lett.*, 2021, **913**, L18.
72 G. Wenzel, S. Gong, C. Xue, P. B. Changala, M. S. Holdren, T. H. Speak, D. A. Stewart, Z. T. P. Fried, R. H. J. Willis, E. A. Bergin, A. M. Burkhardt, A. N. Byrne, S. B. Charnley, A. Lipnicky, R. A. Loomis, C. N. Shingledecker, I. R. Cooke, M. C. McCarthy, A. J. Remijan, A. E. Wendlandt and B. A. McGuire, *Astrophys. J., Lett.*, 2025, **984**, L36.
73 P. Ehrenfreund and J. Cami, *Cold Spring Harbor Perspect. Biol.*, 2010, **2**, a002097.
74 E. K. Campbell, M. Holz and J. P. Maier, *Astrophys. J., Lett.*, 2016, **826**, L4.